American J. of Engineering and Applied Sciences 3 (1): 222-231, 2010
ISSN 1941-7020

Rating of Spur Gear Strength Using Photoelasticity and the Finite Element Method

Konstandinos G. Raptis, Theodore N. Costopoulos,
Georgios A. Papadopoulos and Andonios D. Tsolakis
Laboratory of Machine Elements, Department of Mechanical Engineering,
National Technical University of Athens, Iroon Polytexneiou 9, 15780 Zografou, Greece

Abstract: Problem statement: Toothed gears are some of the most used machine elements for motion and power transmission between rotating shafts. This fact induces the need for improved reliability and higher endurance, which require precise and clear knowledge of the gear tooth stress field during meshing. **Approach:** This study considered the calculation of maximum stress at gear tooth root when the meshing gears are loaded at their most unfavorable contact point (highest point of single-tooth contact-HPSTC), using both numerical and experimental methods. Finite Element Method (FEM) is used for the numerical stress analysis and photoelasticity is applied for the experimental investigation of the stress field. **Results:** The experimental results of the maximum dimensionless stress derived from the photoelasticity experiments are compared to the respective theoretical stress results of the finite element analysis. **Conclusion:** It was found that the deviation between the results of the applied methods falls between reasonable limits whereas it rises with increasing number of teeth of the large gear.

Key words: Spur gears, photoelasticity, Highest Point of Single Tooth Contact (HPSTC), Finite Element Method (FEM)

INTRODUCTION

First systematic attempt to calculate the position of critically stressed point is attributed to Lewis (1882) who considered that the inscribed isosceles parabola tangent to the dedendum of the tooth flank defines the critically stressed point which is located at the point of tangency at the side which is loaded by tensile stresses.

Later, it was observed that the critically stressed point is positioned lower than the one determined by the method of inscribed parabola. This finding is compatible with the photoelasticity experimental results.

The "30 degrees tangent" is another method which argues that the critically stressed point is independent of the load location and it is located at a specific point at the tooth root. Although this method is adopted by the ISO standards, (Kawalec *et al*., 2006), it is approximate and applicable only to low stressed gears.

MATERIALS AND METHODS

Assuming that gear tooth is a stubby cantilever beam, it is derived that the transverse load P_N on a gear tooth is not maximum when applied at the addendum circle as seen at Fig. 1. The complete gear tooth meshing cycle is illustrated in Fig. 2, where tooth meshing, (Spitas and Spitas, 2007; Niemann, 1960), begins at point A and completes at point B with these two points defining the ends of the contact path. It is obvious that between points A and A' and points B and B' two tooth pairs mesh simultaneously. On the other hand, between points A' and B' of contact path, only a single pair of gear teeth is in contact which is subject to the maximum load. The worst loading conditions for the tooth of gear 1 do not occur when the load is applied to the highest addendum point (point B), because the total load is distributed to two pairs of gear teeth at this point, but at point B' of contact path where only a single pair of gear teeth is meshing, (Townsend, 1992; Spitas *et al*., 2006). Point A' defines the Lowest Point of Single Tooth Contact (LPSTC) and point B' is the Highest Point of Single Tooth Contact (HPSTC) for gear 1. In other words, during the portion A'B' of the contact path only a single tooth of each gear is loaded, whereas during portions AA' and BB' the load is distributed to two teeth of each gear. Thus, we can infer that the maximum gear tooth loading occurs at a point on part A'B' of the contact path, (Colbourne, 1987; Costopoulos and Spitas, 2009).

Corresponding Author: Theodore N. Costopoulos, Laboratory of Machine Elements, Department of Mechanical Engineering, National Technical University of Athens, Iroon Polytexneiou 9, 15780 Zografou, Athens Greece

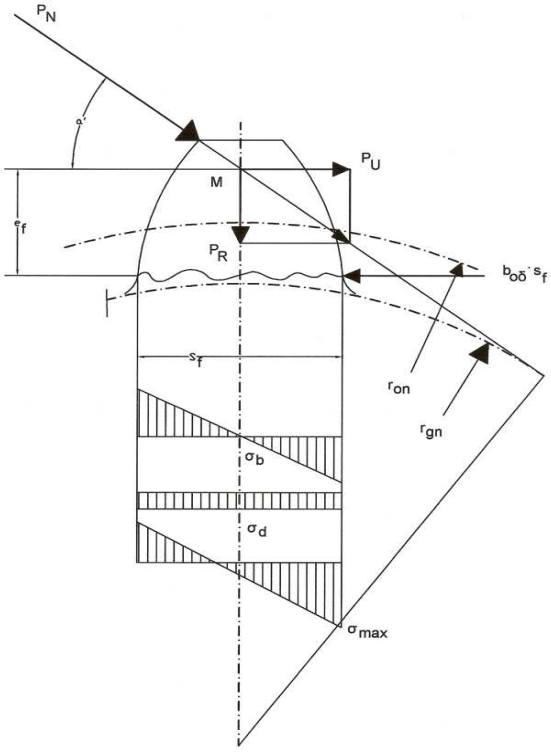

Fig. 1: Gear tooth loading

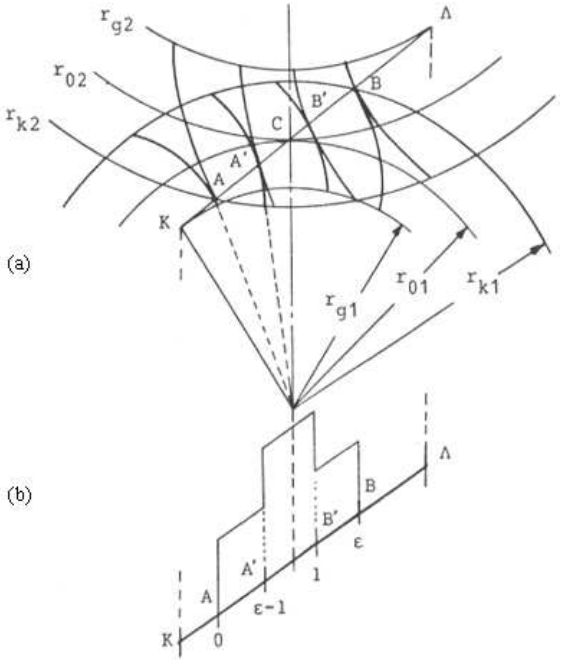

Fig. 2: (a) Meshing teeth profiles of a gear transmission stage; (b) Positions of tooth load variation

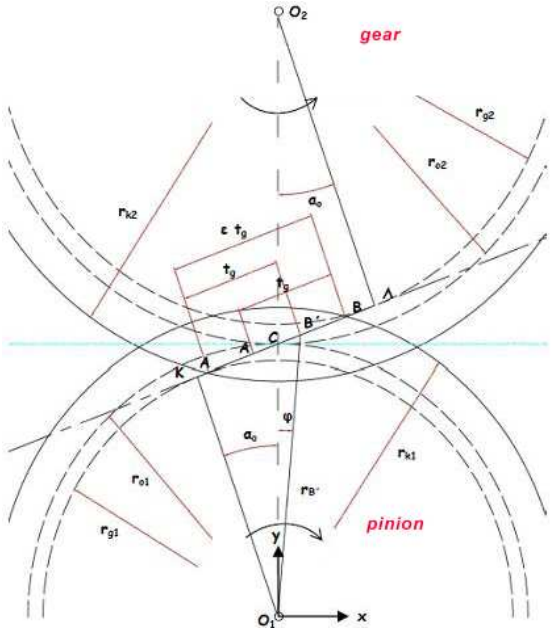

Fig. 3: Geometric determination of HPSTC

Determination of the point of maximum stresses during gear meshing Fig. 3, is as follows:

$$AB = \varepsilon \cdot t_g = AC + CB \tag{1}$$

$$AC = \sqrt{\left(r_{o2} + m\right)^2 - r_{02}^2 \cdot \cos^2 \alpha_o} - r_{02} \cdot \sin \alpha_0 \tag{2}$$

$$BC = \sqrt{\left(r_{01} + m\right)^2 - r_{01}^2 \cdot \cos^2 \alpha_0} - r_{01} \cdot \sin \alpha_0 \tag{3}$$

Substituting Eq. 2 and 3 to Eq. 1 results:

$$AB = \sqrt{\left(r_{o2} + m\right)^2 - r_{02}^2 \cdot \cos^2 \alpha_o} + \sqrt{\left(r_{01} + m\right)^2 - r_{01}^2 \cdot \cos^2 \alpha_0} - \left(r_{01} + r_{02}\right) \cdot \sin \alpha_0 \tag{4}$$

HPSTC is located at point B'. During parts AA' and B'B of the contact path, load is transmitted through two pairs of gear teeth, while during part A'B' only a single pair of gear teeth is subjected to the total load. The lengths of parts AB' and A'B equal the gear circular pitch, t_g, at the base circle. Thus, position of HSPTC is determined according to Fig. 3 as follows:

$$AC = \sqrt{\left(r_{02} + m\right)^2 - r_{02}^2 \cdot \cos^2 \alpha_0} - r_{02} \cdot \sin \alpha_0 \tag{5}$$

$$CB' = AB' - AC = t_g - AC = \pi \cdot m \cdot \cos \alpha_0 - AC \tag{6}$$

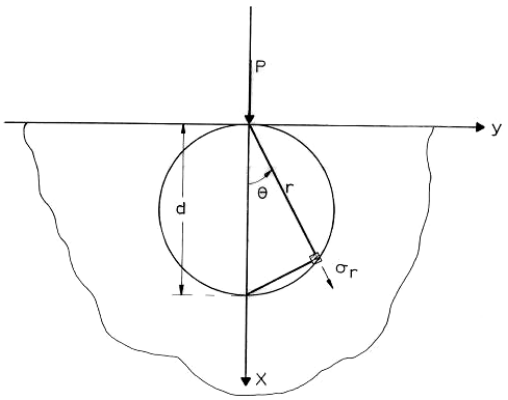

Fig. 4: Geometry of the applied force P at semi-infinite plate

Using triangle $O_1B'C$, radius $r_{B'}$ can be calculated according to (Spitas *et al*., 2005; Spitas *et al*., 2007) by the following equation:

$$r_{B'} = \sqrt{r_{01}^2 + CB'^2 - 2 \cdot r_{01} \cdot CB' \cdot \cos\left(\alpha_0 + 90^0\right)} \quad (7)$$

Cartesian coordinates of point H are: (x, y) = ($r_{B'}$ sinφ, $r_{B'}$ cosφ).

The photoelastic method: A vertical force P acts on a horizontal straight boundary of an infinitely large plate Fig. 4. The stress function, (Timoshenko and Goodier, 1970), is given as:

$$\Phi = -\frac{P}{\pi} \cdot r \cdot \partial \cdot \sin\partial \quad (8)$$

The stresses $\sigma_r, \sigma_\partial, \sigma_{r\partial}$ are given by the relations:

$$\sigma_r = \frac{1}{r}\frac{\partial\Phi}{\partial r} + \frac{1}{r^2}\frac{\partial^2\Phi}{\partial\theta^2} = -\frac{2P}{\pi}\frac{\cos\partial}{r} \quad (9)$$

$$\sigma_\partial = \frac{\partial^2\Phi}{\partial r^2} = 0 \quad (10)$$

$$\sigma_{r\partial} = -\frac{\partial}{\partial r}\left(\frac{1}{r}\frac{\partial\Phi}{\partial\theta}\right) = 0 \quad (11)$$

According to the stress-optical law the difference of the principal stresses is:

$$\sigma = \sigma_1 - \sigma_2 = \frac{N \cdot f_\sigma}{d} \quad (12)$$

Where:
N = The isochromatic fringe order
d = The thickness of the specimens
f_σ = The material fringe value or stress-optical constant

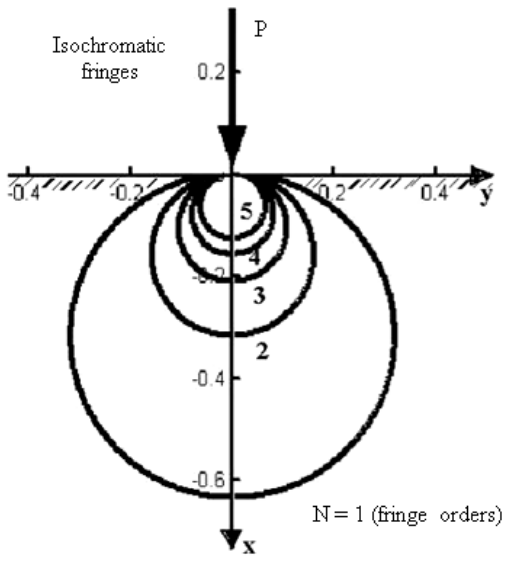

Fig. 5: Isochromatic fringe patterns as they are plotted by the computer.

The stress σ_r, Relation 9, is a principal stress and thus Relation 12 becomes:

$$\frac{2P}{\pi}\frac{\cos\partial}{r} = \frac{N \cdot f_\sigma}{d} \quad (13)$$

or:

$$r = C\frac{\cos\partial}{N} \quad (14)$$

with:

$$C = \frac{2 \cdot d \cdot P}{\pi \cdot f_\sigma} \quad (15)$$

Relation 14 gives the isochromatic fringe patterns. Fig. 5 presents the isochromatic fringe patterns which were plotted according to Relation 14.

For a disk of diameter D the difference, $\sigma = \sigma_1 - \sigma_2$, of principal stresses at the center of the disk is given by:

$$\sigma = \sigma_1 - \sigma_2 = \frac{8 \cdot P}{\pi \cdot d \cdot D} \quad (16)$$

and Relation 16 becomes:

$$P = \frac{N \cdot \pi \cdot f_\sigma \cdot D}{8} \quad (17)$$

Relation 17 gives the compressive load P at the center of the disk, or the stress-optical constant $f_{\sigma,}$ if the compressive load is given.

Dimensionlessness of stresses: Using the concept of dimensionless stress, proposed by (Townsend, 1992; Spitas *et al*., 2006), according to Eq. 18, we can compare the experimental results of photoelasticity to the respective stresses resulting from the finite element analyses, which have first to be reduced to a dimensionless form:

$$\sigma_u = \sigma\frac{b\cdot m}{P} = \sigma\frac{b\cdot m\cdot \cos\alpha'}{P_u} \quad (18)$$

Here:

σ_u = Dimensionless stress
σ = Calculated (real) stress (MPa)
b = Gear tooth length (m)
m = Module of gearing (m)
P = Transverse load to the gear tooth at HPSTC (N)
P_u = Horizontal component of the previous load (normal to the axis of symmetry of the gear tooth) (N)
α' = Angle between the line of action of the load and the horizontal (°)

The advantage of this consideration is that at all cases both the gear module (m) and the gear tooth length (b) are equal to unity, while at the same time a unit load (P = 1) is assumed at HPSTC. Thus, after the calculation of the maximum dimensionless stress using Eq. 18 assuming particular values for the gear tooth length, the module of gearing and tooth loading of a gear reduction stage, we are able to calculate the real stress for any value of each of the these three variable parameters. Therefore for this gear stage, useful results can be extracted faster by using this time-saving method.

Photoelasticity experiments: Four specimens were manufactured simulating standard gears having 15, 18, 22 and 28 teeth, respectively. A gear module of 20 mm and gear tooth length, b, of 9.25 mm were chosen (Fig. 6-9). Specimen material is PSM-1 with Young modulus E = 2.5 GPa and Poisson ratio ν = 0.38.

Using the cyclic polariscope of Fig. 10 with loading at HPSTC, the maximum stresses were determined experimentally for each pair of the previous gear tooth specimens, according to Table 1. Initially each gear tooth is loaded with a 22.240 N (5 lb) force. Then, the load increases gradually until a fringe of integer order emerges at the critical point, first under monochromatic light and next under white light, as shown in Fig. 11-26.

Table 1: HPSTC specimen tests

Test No.	No. of teeth of gear 1	No. of teeth of gear 2	Distance between HPSTC and specimen base (mm)
Standard gears			
1	15	18	72.75
2	18	15	72.07
3	15	22	72.10
4	22	15	70.97
5	15	28	71.39
6	28	15	69.98
7	18	22	70.84
8	22	18	70.38

Fig. 6: Specimen of a standard gear with 15 teeth

Fig. 7: Specimen of a standard gear with 18 teeth

Fig. 8: Specimen of a standard gear with 22 teeth

Fig. 9: Specimen of a standard gear with 28 teeth

Fig. 10: Polariscope and specimen loading apparatus for the photoelasticity experiments installed at the NTUA Machine Elements Laboratory

Fig. 11: Test No. 1 (15/18)-pinion-monochromatic light

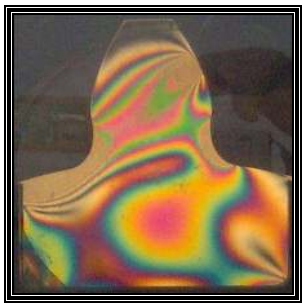

Fig. 12: Test No. 1 (15/18)-pinion-white light

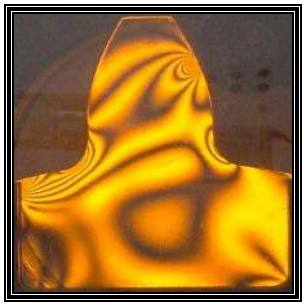

Fig. 13: Test No.2-(15/18)-gear-monochromatic light

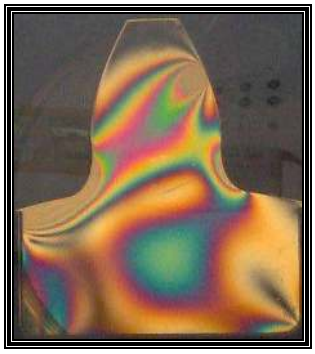

Fig. 14: Test No. 2-(15/18)-gear-white light

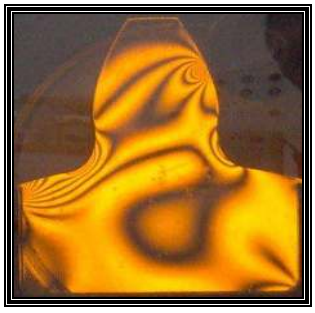

Fig. 15: Test No. 3-(15/22)-pinion-monochromatic light

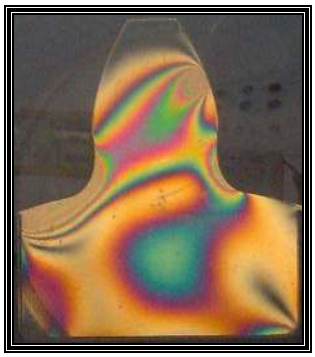

Fig. 16: Test No. 3-(15/22)-pinion-white light

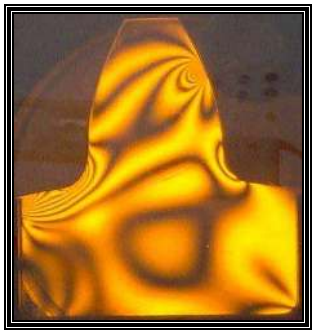

Fig. 17: Test No. 4-(15/22)-gear-monochromatic light

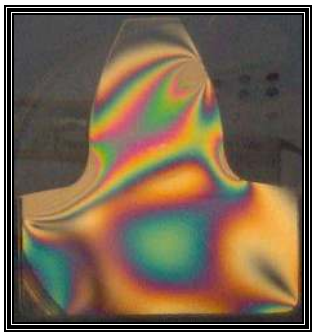

Fig. 18: Test No. 4-(15/22)-gear-white light

Fig. 19: Test No. 5-(15/28)-pinion-monochromatic light

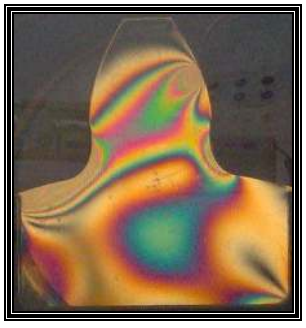

Fig. 20: Test No. 5-(15/28)-pinion-white light

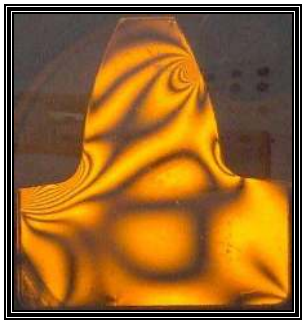

Fig. 21: Test No. 6-(15/28)-gear-monochromatic light

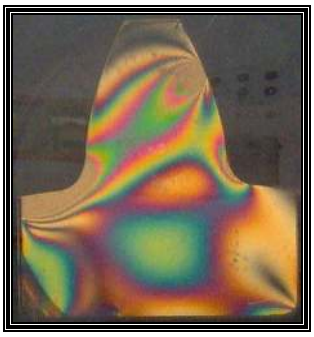

Fig. 22: Test No. 6-(15/28)-gear-white light

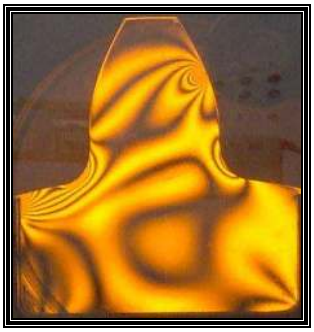

Fig. 23: Test No. 7-(18/22)-pinion-monochromatic light

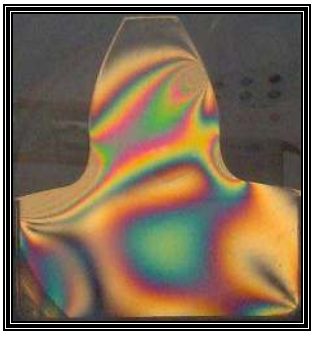

Fig. 24: Test No. 7-(18/22)-pinion-white light

Table 2: Experimental estimations of maximum stresses of the specimens

Test No.	HPSTC horizontal load, P_u (lbs)	HPSTC horizontal load, P_u (N)	Isochromatics order,	Maximum stress, σ (MPa)
Standard gears				
1	55.0	244.652	3	4.572
2	38.5	171.257	2	3.048
3	37.5	166.808	2	3.048
4	41.0	182.377	2	3.048
5	38.0	169.032	2	3.048
6	43.5	193.498	2	3.048
7	40.0	177.929	2	3.048
8	41.5	184.601	2	3.048

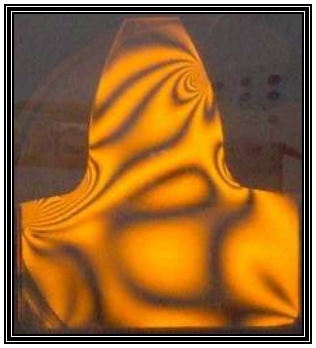

Fig. 25: Test No. 8-(18/22)-gear-monochromatic light

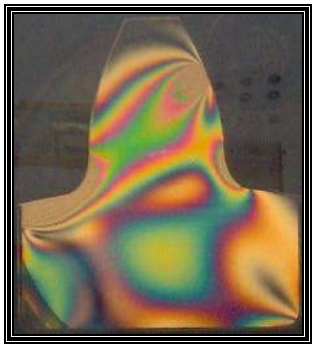

Fig. 26: Test No. 8-(18/22)-gear-white light

Subsequently, for the loading at HPSTC, maximum stresses were estimated by using Eq. 12. Table 2 contains the results of these calculations.

Gear tooth modeling and stress analysis using the finite element method: Gear models with 15, 18, 22 and 28 teeth, module of 20 mm and gear tooth length of b = 9.25 mm were created at Autodesk Inventor CAD system, using common geometry and material properties of the photoelasticity specimens.

Next, the HPSTC positions were determined for gear pair, using Eq. 5-7. Results are shown in Table 3.

Table 3: HPSTC positions of all gears

Test No.	Number of teeth for gear 1	Number of teeth for gear 2	Distance between HPSTC and the tooth center (mm)
Standard gears			
1	15	18	155.297
2	18	15	185.794
3	15	22	154.672
4	22	15	225.695
5	15	28	153.983
6	28	15	285.598
7	18	22	184.600
8	22	18	225.126

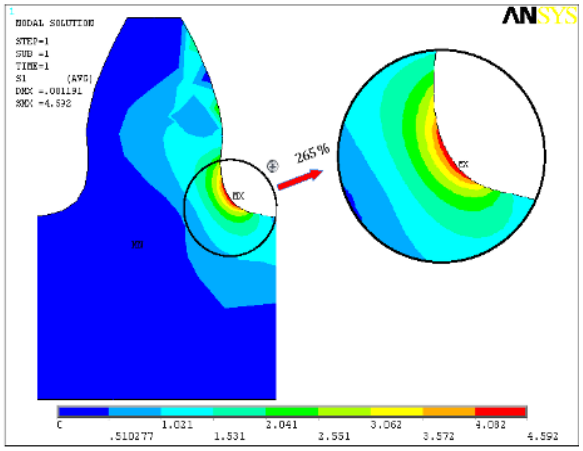

Fig. 27: Test No. 1-15/18-pinion-stress field

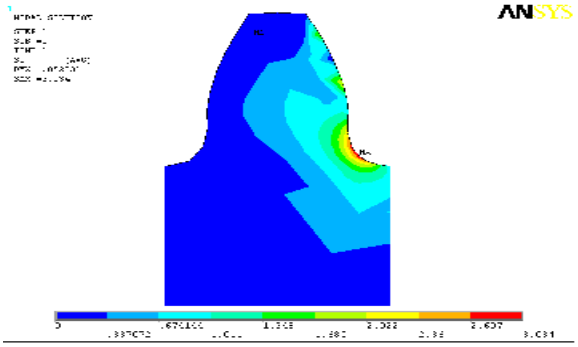

Fig. 28: Test No. 2-15/18-gear -stress field

CAD models are imported to the ANSYS environment. The applied loads P_u are adapted from the experimental results, Table 2. Taking into account the angle α' between the line of load action and the horizontal line, shown in Fig.1, it is clear that this angle is different for each tooth pair. Then the total load of each gear tooth pair is found, as shown in Table 4.

After the total load has been applied to the gear tooth finite element models in ANSYS environment, we can find the maximum stresses, σ_{max}, for each case, as shown schematically in Fig. 27-34.

Table 4: Loads applied to HPSTC of gear tooth finite element models

Test No.	No. of teeth for gear 1	No. of teeth for gear 2	Angle between the line of load and the horizontal, α'(°)	Horizontal component of HPSTC,P_u(N)	Total load (normal to great tooth flank) at HPSTC, P(N)
Standard gears					
1	15	18	19.610	244.652	259.716
2	18	15	20.116	171.257	182.382
3	15	22	19.091	166.808	176.517
4	22	15	20.116	182.377	194.225
5	15	28	18.377	169.032	178.116
6	28	15	20.116	193.498	206.068
7	18	22	19.265	177.929	188.484
8	22	18	19.780	184.601	196.176

Table 5: Numerical results for maximum tooth stresses

Test No.	Total load, P (N)	Maximum stress, σ_{max} (MPA)
Standard gears		
1	259.716	4.592
2	182.382	3.034
3	176.517	3.076
4	194.225	3.101
5	178.116	2.942
6	206.068	3.160
7	188.484	3.092
8	196.176	3.047

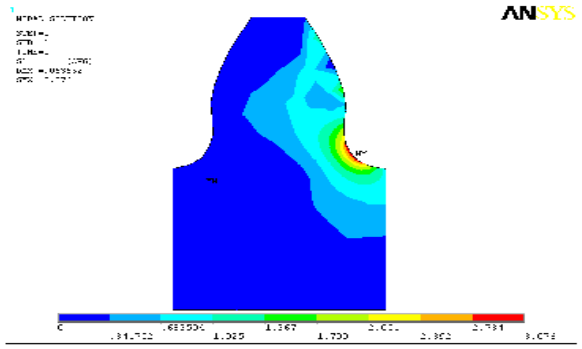

Fig. 29: Test No. 3-15/22-pinion-stress field

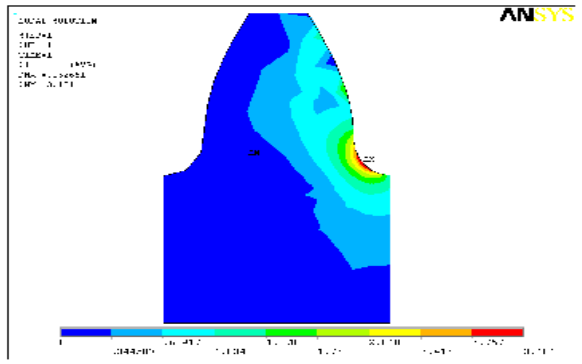

Fig. 30: Test No. 4-15/22-gear-stress field

Table 5 assembles the numerical results of the stress analyses. Afterwards, by using Eq. 18, experimental and numerical values of maximum stresses, Table 6, become dimensionless in order to become comparable, (Table 7).

Table 6: Experimental and numerical estimations of maximum gear tooth stresses

Test No.	Total load at HPSTC, P(N)	Experimental estimation of maximum tooth stress, σ_π(MPA)	Numerical estimation of maximum tooth stress, σ_θ(MPA)
Standard gears			
1	259.716	4.572	4.592
2	182.382	3.048	3.034
3	176.517	3.048	3.076
4	194.225	3.048	3.101
5	178.116	3.048	2.942
6	206.068	3.048	3.160
7	188.484	3.048	3.092
8	196.176	3.048	3.047

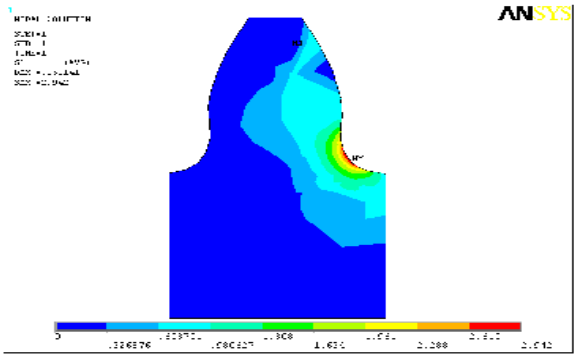

Fig. 31: Test No. 5-15/28-pinion-stress field

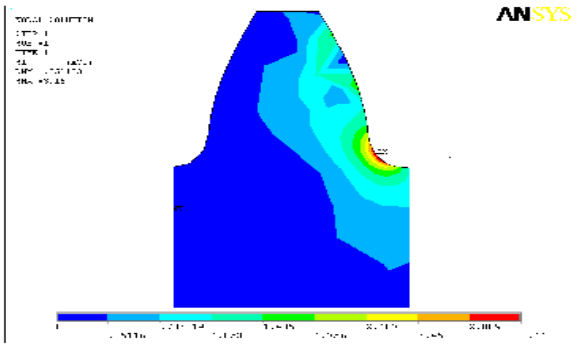

Fig. 32: Test No. 6-15/28-gear-stress field

Table 7: Deviation between experimental and numerical estimations of maximum dimensionless stresses

Test No.	No. of teeth for gear 1	No. of teeth for gear 2	Experimental estimation of maximum dimensionless stress, $\sigma_{u\pi}$	Numerical estimation of maximum dimensionless stress, $\sigma_{u\theta}$	Deviation between the estimations of the two methods (5)
Standard gears					
1	15	18	3.257	3.271	-0.4
2	18	15	3.092	3.078	0.5
3	15	22	3.194	3.224	-0.9
4	22	15	2.903	2.954	-1.7
5	15	28	3.166	3.056	3.6
6	28	15	2.736	2.837	-3.5
7	18	22	2.992	3.035	-0.4
8	22	18	2.874	2.873	0.0

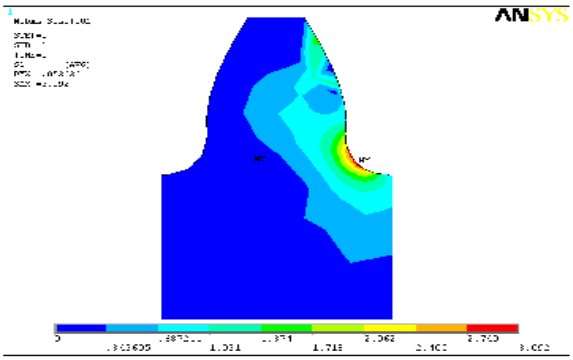

Fig. 33: Test No. 7-18/22-pinion-stress field

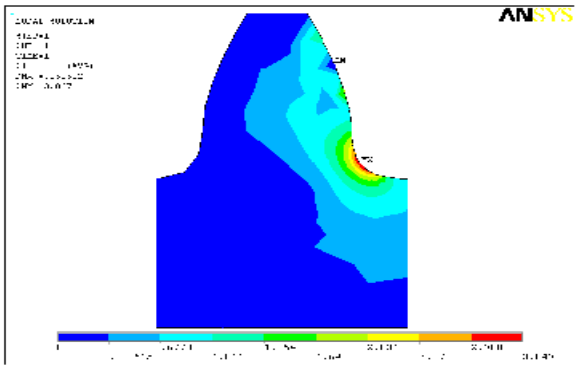

Fig. 34: Test No. 8-18/22-gear-stress field

RESULTS

If we compare the results in Table 7, we can see that there is deviation of the maximum stress estimation from -3.5% to +3.6% between the experimental and the numerical methods. This deviation increases with the number of teeth of the bigger gear, keeping constant the number of pinion teeth.

DISCUSSION

Apart from the fatigue failure at the critically stressed point, small cracks at tooth surface have been observed at gear pitch circle (where the gear tooth is subjected to the total load), due to high pressure surface fatigue. Low viscosity lubricants can enter the cracks at high pressures. These initially small cracks can easily grow under the effect of high pressures of penetrating fluids, causing surface fatigue cracks or pitting. Therefore, it is critical to take into account the surface fatigue strength of gear during the design procedure.

CONCLUSION

In this study, the minimum deviation between the results of the applied methods was investigated. Results of photoelasticity experiments, which is the most widely applied experimental method for gear stress analysis, were compared to the results of the finite elements method using ANSYS software. Comparison of the results of the two applied methods proved that the deviations are acceptable. These deviations are reasonable considering the potential errors that can be involved during the application of the two methods.

REFERENCES

Colbourne, J., 1987. The Geometry of Involute Gears. Springer-Verlag, ISBN: 0-387-96522-X, pp: 253.

Costopoulos, T. and V. Spitas, 2009. Reduction of gear fillet stresses by using asymmetric teeth. J. Mechan. Mach. Theor., 44: 1524-1534. DOI: 10.1016/j.mechmachtheory.2008.12.002

Kawalec, A., J. Wiktor and D. Ceglarek, 2006. Comparative analysis of tooth-root strength using ISO and AGMA standards in spur and helical gears with FEM-based verification. J. Mech. Des., 128: 1141-1158. DOI: 10,1115/1.2214735

Lewis, W., 1882. Investigation of the strength of gear teeth. Proceedings of the Engineering Club No. I, (EC'82), Philadelphia, pp: 16-23.

Niemann, G., 1960. Maschinenelemente II. Springer-Verlag, ISBN: 3-540-03378-5, pp: 97.

Spitas, V., Th. Costopoulos and C. Spitas, 2005. Increasing the strength of standard involute gear teeth with novel circular root fillet design. Am. J. Applied Sci., 2: 1058-1064. http://www.scipub.org/fulltext/ajas/ajas261058-1064.pdf

Spitas, V., T. Costopoulos and C. Spitas, 2006. Optimum gear tooth geometry for minimum fillet stress using BEM and experimental verification with photoelasticity. J. Mech. Des., 128: 1159-1164. DOI: 10,1115/1.2216731

Spitas, V. and C. Spitas, 2007. Numerical and experimental comparative study of strength optimized AGMA and FZG spur gears. Acta Mech., 193: 113-126. DOI: 10.1007/s00707-006-0384-x

Spitas, V., T. Costopoulos, and C. Spitas, 2007. Fast modeling of conjugate gear tooth profiles using discrete presentation by involute segments. J. Mechan. Mach. Theor., 42: 751-762. DOI: 10.1016/j.mechmachtheory.2006.05.007

Timoshenko, S. and J. Goodier, 1970. Theory of Elasticity. McGraw-Hill, ISBN: 0-07-0858053, pp: 301.

Townsend, D.P., 1992. Dudley's Gear Handbook. 2nd Edn., McGraw Hill, ISBN: 0-07-017903-4, pp: 611.